Characterization of Organically Modified Clays Using Scattering and Microscopy Techniques

Derek L. Ho,*,†,‡ Robert M. Briber,† and Charles J. Glinka‡

Department of Materials and Nuclear Engineering, University of Maryland, College Park, Maryland 20742, and Center for Neutron Research, National Institute of Standards and Technology, Gaithersburg, Maryland 20899

Received October 31, 2000. Revised Manuscript Received February 27, 2001

Understanding the structure of organophilic clays and the interaction between clay platelets dispersed in organic solvents is important for characterizing nanocomposites formed by organophilic clays and polymers. To understand and optimize potential processing conditions, organically modified montmorillonite clays were dispersed in a number of organic solvents covering a range of solubility parameters and characterized using small-angle neutron scattering and wide-angle X-ray scattering techniques. The organic modifier was dimethyl dihydrogenated tallow ammonium. Both as-received (unextracted) and purified (extracted) organically modified clays were studied. The scattering profiles and dispersion behavior in organic solvents of the dry powder of unextracted and of extracted dimethyl dihydrogenated tallow montmorillonite are significantly different, confirming that the organic modifiers are present in excess in the unextracted material as reported by the industrial provider. The scattering data show that both unextracted and extracted organically modified clay platelets were fully exfoliated in chloroform while the platelets retain their lamellar structure and swell to a similar extent in benzene, toluene, and *p*-xylene, but the extracted material has a stronger tendency to gel. The scattering profiles indicate that the swollen tactoids of extracted material are thinner, and therefore more numerous, which may account for the bulk suspension behavior. The extracted clay dispersion exhibited a concentration dependence on the scattering for all the organic solvents studied except chloroform while the unextracted clay dispersion did not. Neither the extracted nor the unextracted dispersions exhibited any temperature dependence on the scattering. The thickness of unmodified montmorillonite platelets was found to be 9.9 Å while that of organically modified montmorillonite platelets was determined to be 24.3 Å using wide-angle X-ray scattering. The lateral size of organically modified montmorillonite platelets was observed to be in the range of 0.4−1.0 μm using atomic force microscopy.

Introduction

Sodium montmorillonite (Na^+−montmorillonite), a natural clay mineral, has been studied extensively by diffraction techniques.[1−4] More recently, it has been used to form nanocomposites with polymers with significantly enhanced mechanical properties.[5−9] Na^+−montmorillonite, a smectite clay, is a hydrophilic mineral, which possesses a 2-to-1 layered structure with a single octahetral aluminum layer located between two layers of silicon tetrahedra, and has a nominal chemical formula of $[(Al_{1.67}Mg_{0.33})Si_4O_{10}(OH)_2]Na_{0.33}\cdot nH_2O$, which varies depending on the source of clay.[1−3] Each layered sheet is about 10-Å thick with literature lateral dimensions of 0.1 μm to more than 1 μm. This yields a specific surface area of ca. 725 m^2/g.[1] Through chemical substitution on the surface, clays of Na^+−montmorillonite can be modified to convert the surface from hydrophilic to organophilic, resulting in clays that are dispersible in common organic solvents. Typically, this is accomplished via a cationic substitution reaction with the surface sodium ion.[4] Organic cations may be adsorbed on clay minerals by replacement of the inorganic metal ions saturating the structural negative charge on the silicate layers.

Although small-angle neutron scattering (SANS) has been recently used to characterize a variety of unmodified clays dispersed in water[10−12] as well as nanocomposites formed by clays and polymers in water-based

* To whom correspondence should be addressed.
† University of Maryland.
‡ National Institute of Standards and Technology.

(1) Theng, B. K. G. *Formation and Properties of Clay-Polymer Complexes*; Elsevier: New York, 1979.
(2) Worrall, W. E. *Clays*; Transatlantic Arts: New York, 1968.
(3) Chamley, H. *Clay Sedimentology*; Springer-Verlag: New York, 1989.
(4) Newman, A. C. D. *Chemistry of Clays and Clay Minerals*; Wiley: New York, 1987.
(5) Krishnamoorti, R.; Vaia, R. A.; Giannelis, E. P. *Chem. Mater.* **1996**, *8*, 1728.
(6) Giannelis, E. P.; Krishnamoorti, R.; Manias, E. *Adv. Polym. Sci.* **1999**, *138*, 108−147.
(7) LeBaron, P. C.; Wang, Z.; Pinnavaia, T. J. *Appl. Clay Sci.* **1999**, *15*, 11−29.
(8) Krishnamoorti, R.; Giannelis, E. P. *Macromolecules* **1997**, *30*, 4097.
(9) Mourchid, A.; Lecolier, E.; Van Damme, H.; Levitz, P. *Langmuir* **1998**, *14*, 4718.

10.1021/cm0008617 CCC: $20.00
Published on Web 04/28/2001

systems,[13,14] relatively few attempts have been made to investigate organically modified clays dispersed in common organic solvents by scattering techniques. Thus, the motivation of this work is to study the behavior of organically modified clays in a variety of organic solvents using SANS and wide-angle X-ray scattering (WAXS) techniques as well as to characterize the lateral size of organically modified clay platelets using atomic force microscopy (AFM).

Experimental Section

Cloisite Na^+ (CNa), a sodium montmorillonite (Na^+−montmorillonite), and Cloisite 15A (C15A), a substituted dimethyl dihydrogenated tallow montmorillonite, used in this work are commercial products provided as a free-flowing powder by Southern Clay Products, Inc.[15] C15A was synthesized by ion-exchanging CNa clays with a cation-exchange capacity (CEC) of 1.25 mequiv/g with dimethyl dihydrogenated tallow ammonium. Because the CEC of CNa clays is estimated to be 0.92−0.95 mequiv/g, the surface of C15A is covered by about 130% of one CEC layer.[16] The ditallow is a mixture of dimethylammonium surfactants with various carbon chain lengths of ca. 65% of C_{18}, 30% of C_{16}, and 5% of C_{14}.[16,17] The C_{18} chain has an estimated chain length of ca. 26.7 Å with an all trans structure when fully stretched.

Prior to SANS and WAXS experiments, the as-received CNa was fractionated by sonicating the platelets in deionized water at a mass fraction of 2 wt % for 2 min with an ultrasound probe (General Electric; GE375)[15] to narrow the distribution in particle size of the CNa clay platelets. The small fraction (fraction 1) was separated as a sediment by centrifuging the dispersion at 5000 rpm (International Equipment Co.; Clinical Centrifuge)[15] for 20 min and discarded. The supernatant was then centrifuged at 7000 rpm for 20 min to obtain the second fraction (fraction 2), which contained most of the remaining clay. Fraction 2 was dried in an oven under vacuum at room temperature for 3 days and used in the experiments. To remove excess dimethyl dihydrogenated tallow from the as-received (unextracted) C15A, the unextracted C15A powder was purified by refluxing with hot ethyl alcohol, which was replaced once daily, for 3 days. The purified (extracted) C15A sample was then dried in an oven under vacuum at room temperature for 3 days. The unextracted and extracted C15A clays were then dispersed in chloroform, benzene, toluene, *p*-xylene, cyclohexane, and octane by sonicating the mixtures for 2 min.

The solubility parameters (δ) for chloroform, benzene, toluene, *p*-xylene, cyclohexane, and octane are 19.0, 18.8, 18.2, 18.0, 16.8, and 15.6 $(J/m^3)^{1/2}$, respectively,[18] and the literature value of δ for tallow[17] is in the range from 18 to 28 $(J/m^3)^{1/2}$. It was found that in benzene, toluene, or *p*-xylene the unextracted C15A platelets could be dispersed at 2 wt % to yield a transparent liquid dispersion while the extracted C15A formed a transparent gel suspension under the same conditions. In chloroform, the unextracted C15A platelets were dispersed at 2 wt % to yield a cloudy liquid dispersion while the extracted C15A formed a cloudy gel suspension. In cyclohexane or octane, the dispersion of the unextracted clay appeared to be cloudy while the extracted clay precipitated. Video-enhanced differential interference contrast (DIC) optical microscopy images taken on the cloudy dispersions and the precipitates of unextracted and extracted C15A clay platelets, respectively, in cyclohexane and octane confirm that the platelets aggregated to form large particles. Table 1 summarizes the solubility parameter (δ) of the organic solvents[18] used in this work and the appearance of C15A dispersed in the solvents.

Table 1. Solvent Solubility Parameter and C15A Dispersion Appearance

solvent	δ^a/ $(J/m^3)^{1/2}$	2 wt % extracted	2 wt % unextracted
chloroform	19.0	cloudy gel	cloudy dispersion
benzene	18.8	transparent gel	transparent dispersion
toluene	18.2	transparent gel	transparent dispersion
p-xylene	18.0	transparent gel	transparent dispersion
cyclohexane	16.8	precipitates	cloudy dispersion
octane	15.6	precipitates	cloudy dispersion

[a] δ represents the solubility parameter.

SANS experiments over the q range from 0.004 to 0.517 $Å^{-1}$ were carried out using the 30-m SANS instruments at the National Institute of Standards and Technology (NIST) Center for Neutron Research (NCNR).[19] The incident neutron wavelength was $\lambda = 6$ Å with a wavelength resolution of $\Delta\lambda/\lambda = 0.11$. The scattered intensity was corrected for background and parasitic scattering,[20] placed on an absolute level using a calibrated secondary standard and circularly averaged to yield the scattered intensity, $I(q)$, as a function of the wave vector, q, where $q = (4\pi/\lambda)\sin(\theta/2)$ (θ is the scattering angle). The incoherent background from the pure solvents was measured, corrected by the volume fraction displaced by the dispersed clay, and subtracted from the reduced SANS data. The data points in the q range from 0.35 to 0.45 $Å^{-1}$ were then averaged to yield the estimated incoherent background from clays, which was subtracted from the data as well. WAXS measurements were performed at room temperature over the q range from 0.07 to 1.07 $Å^{-1}$ using Ni-filtered Cu Kα X-rays of wavelength $\lambda = 1.54$ Å.

SANS and WAXS measurements were performed on the dry powders of unextracted and of extracted C15A, the dispersions of unextracted C15A in all the deuterated (d-) versions of the solvents noted above at 2 wt %, and the dispersions of extracted C15A in d-chloroform, d-benzene, d-toluene, and d-*p*-xylene at 1 wt % concentration. SANS contrast variation experiments were also carried out on the dispersions of extracted C15A in deuterated/protonated (d/h) *p*-xylene mixtures at concentrations of ca. 0.1 and 1 wt % as well as on the dispersions of centrifuged CNa in a range of deuterated/protonated water (D_2O/H_2O) at a concentration of ca. 1 wt % at room temperature. SANS and WAXS measurements on dry powders of as-received and of centrifuged CNa were also performed.

To quantitatively characterize the lateral size of C15A clay platelets using AFM, extracted C15A thin layers were spun from a dispersion of extracted C15A in *p*-xylene at 1 wt % onto 1-in.-diameter silicon (Si) wafers (ca. 0.02-cm thick). Prior to spinning, the Si wafers were cleaned in chromerge at 80 °C for 3 h to remove any organic residuals on the surface, etched

(10) Ramsay, J. D. F.; Swanton, S. W.; Bunce, J. *J. Chem. Soc., Faraday Trans.* **1990**, *86*, 3919.
(11) Ramsay, J. D. F.; Lindner, P. *J. Chem. Soc., Faraday Trans.* **1993**, *89*, 4207.
(12) Brown, A. B. D.; Clarke, S. M.; Rennie, A. R. *Prog. Colloid Polym. Sci.* **1998**, *110*, 80.
(13) Jinnai, H.; Smalley, M. V.; Hashimoto, T. *Langmuir* **1996**, *12*, 1199.
(14) Hatharasinghe, H. L. M.; Smalley, M. V.; Swenson, J.; Williams, G. D.; Heenan, R. K.; King, S. M. *J. Phys. Chem. B* **1998**, *102*, 6804.
(15) Certain commercial materials and equipment are identified in this paper to specify adequately the experimental procedure. In no case does such identification imply recommendation by the National Institute of Standards and Technology nor does it imply that the material or equipment identified is necessarily the best available for this purpose.
(16) Material Safety Data Sheets provided by Southern Clay Products, Inc. and Akzo Nobel Chemicals, Inc.
(17) Fasman, G. D. *Practical Handbook of Biochemistry and Molecular Biology*; CRC Press: New York, 1989.
(18) Barton, A. F. M. *CRC Handbook of Polymer-Liquid Interaction Parameters and Solubility Parameters*; CRC Press: New York, 1990.
(19) Glinka, C. J.; Barker, J. G.; Hammouda, B.; Krueger, S.; Moyer, J. J.; Orts, W. J. *J. Appl. Crystallogr.* **1998**, *31*, 430.
(20) Cold Neutron Research Facility at the National Institute of Standards and Technology. *NG3 and NG7 30-Meter SANS Instruments Data Acquisition Manual*, 1999.

using hydrofluoric (HF) acid to remove the SiO_2 layer on the surface, and thoroughly rinsed with deionized water. Tapping mode AFM (Digital Instrument; Dimension 3100)[15] was used to image the spun extracted C15A platelets on the Si wafers. The AFM was operated in tapping mode under ambient conditions with commercial silicon microcantilever probe tips. Manufacturer's values for the probe tip radius and probe spring constant are in the range of 5−10 nm and of 20−100 N/m, respectively. Topographic and phase images were obtained simultaneously using a resonance frequency of approximately 300 kHz for the probe oscillation and a free-oscillation amplitude of (60 ± 5) nm. A set-point ratio (r_{sp}) in the range of 0.65−0.75 was used.

Theoretical

The CNa platelets can be modeled as individual thin circular disks, that is, flat cylinders, with a thickness of ca. 10 Å and a diameter of ca. 0.4−1 μm. For monodisperse noninteracting CNa clay platelets in a dilute suspension, the total coherent scattered intensity, which is isotropic, is given by[21−23]

$$I^{\mathrm{CNa}}_{\mathrm{Single}}(q) = (\Delta\rho_{\mathrm{CNa}})^2 N_{\mathrm{CNa}} V_{\mathrm{CNa}}{}^2 \int_0^{\pi/2} \left(\frac{\sin(qh\cos\varphi)}{qh\cos\varphi}\right)^2 \times \left(\frac{2J_1(qR\sin\varphi)}{qR\sin\varphi}\right)^2 \sin\varphi\, \mathrm{d}\varphi$$

$$\equiv (\Delta\rho_{\mathrm{CNa}})^2\, \phi_{\mathrm{CNa}} V_{\mathrm{CNa}} P_{\mathrm{CNa}}(q) \quad (1)$$

where $2h$ is the axial length (thickness) of the disks, R is the radius, and $P(q)$ is the single platelet form factor. φ is the angle between q and the axis of the disk and $J_1(x)$ is the first-order Bessel function. ϕ_{CNa}, N_{CNa}, and V_{CNa} represent the volume fraction of the CNa clays, the number of CNa clay platelets per unit volume, and the volume of single CNa clay platelets. ρ_i is the neutron scattering length density (SLD) of species i and $\Delta\rho_{\mathrm{CNa}} = \rho_{\mathrm{CNa}} - \rho_{\mathrm{solvent}}$ is the corresponding scattering contrast with respect to the solvent.

For the C15A clay platelets, assuming that the radius of the platelets does not change upon adsorption of a tallow layer (surfactant) and that the only change is in the thickness of the platelet, the simplest model is that of a lamellar clay/tallow (core/layer) structure[24−26] as illustrated in Figure 1a. Assuming the neutron SLD of core and of layer are homogeneous in the $x-y$ plane, as shown in Figure 1a,b, the coherent scattered intensity from such a core/layer structure is determined by the core and layer neutron SLD profiles, $\rho_{\mathrm{core}}(z) \equiv \rho_{\mathrm{c}}$ and $\rho_{\mathrm{layer}}(z) \equiv \rho_{\mathrm{l}}$ and by the corresponding scattering contrast, $\Delta\rho_{\mathrm{c,l}} = \rho_{\mathrm{c,l}} - \rho_{\mathrm{solvent}}$. The total coherent scattered intensity from randomly oriented individual C15A clay platelets with a core of volume $V_{\mathrm{c}} = (\pi R^2)(2h)$ and a total platelet volume of $V_{\mathrm{t}} = (\pi R^2)[2(d + h)]$, where R, $2h$, and d are the radius, the core thickness, and the average thickness of the surfactant layer on each side of a clay platelet, respectively, can be written in the form[24,26]

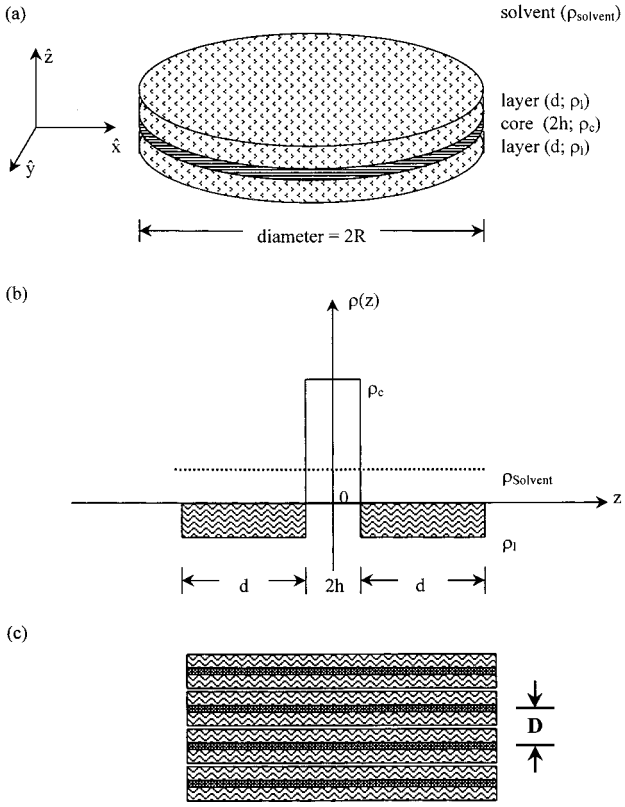

Figure 1. (a) Schematic of the structure of an individual clay/tallow (core/layer) C15A clay platelet. (b) The corresponding neutron scattering length density profiles $\rho(z)$ perpendicular to the platelet plane. (c) Schematic of clay platelets present in tactoids.

$$I^{\mathrm{C15A}}_{\mathrm{Single}}(q) = N_{\mathrm{C15A}} \int_0^{\pi/2} [\Delta\rho_1(V_{\mathrm{t}} f_{\mathrm{t}}(q) - V_{\mathrm{c}} f_{\mathrm{c}}(q)) + \Delta\rho_{\mathrm{c}} V_{\mathrm{c}} f_{\mathrm{c}}(q)]^2 \sin\varphi\, \mathrm{d}\varphi \quad (2)$$

where $\langle f_{\mathrm{t}}{}^2(q)\rangle_\varphi = P_{\mathrm{t}}(q)$ and $\langle f_{\mathrm{c}}2(q)\rangle_\varphi = P_{\mathrm{c}}(q)$ represent the single-particle form factor for the total C15A clay platelet and the core (CNa clay platelet), respectively, and N_{C15A} denotes the number of C15A clay platelets per unit volume.

$$P_{\mathrm{c}}(q) = \int_0^{\pi/2} \left[\left(\frac{\sin(qh\cos\varphi)}{qh\cos\varphi}\right) \times \left(\frac{2J_1(qR\sin\varphi)}{qR\sin\varphi}\right)\right]^2 \sin\varphi\, \mathrm{d}\varphi \quad (3a)$$

$$P_{\mathrm{t}}(q) = \int_0^{\pi/2} \left[\left(\frac{\sin(q(d+h)\cos\varphi)}{q(d+h)\cos\varphi}\right) \times \left(\frac{2J_1(qR\sin\varphi)}{qR\sin\varphi}\right)\right]^2 \sin\varphi\, \mathrm{d}\varphi \quad (3b)$$

$$P_{\mathrm{t,c}}(q) = \int_0^{\pi/2} \left(\frac{\sin(q(d+h)\cos\varphi)}{q(d+h)\cos\varphi}\right)\left(\frac{\sin(qh\cos\varphi)}{qh\cos\varphi}\right) \times \left(\frac{2J_1(qR\sin\varphi)}{qR\sin\varphi}\right)^2 \sin\varphi\, \mathrm{d}\varphi \quad (3c)$$

Equations 1 and 2 introduced are the single-platelet form factors for CNa and C15A clay platelets, respec-

(21) Guinier, A.; Fournet, G. *Small Angle Scattering of X-rays*; Wiley: New York, 1955.
(22) Kratky, O.; Porod, G. *J. Colloid Sci.* **1949**, *4*, 35.
(23) Higgins, J. S.; Benoit, H. C. *Polymers and Neutron Scattering*; Clarendon Press: Oxford, 1994.
(24) Bongiovanni, R.; Ottewill, R. H.; Rennie, A. R. *Prog. Colloid Polym. Sci.* **1991**, *84*, 299.
(25) Richter, D.; Schneiders, D.; Monkenbusch, M.; Willner, L.; Fetters, L. J.; Huang, J. S.; Lin, M.; Mortensen, K.; Farago, B. *Macromolecules* **1997**, *30*, 1053.
(26) Hanley, H. J. M.; Muzny, C. D.; Butler, B. D. *Langmuir* **1997**, *13*, 5276.

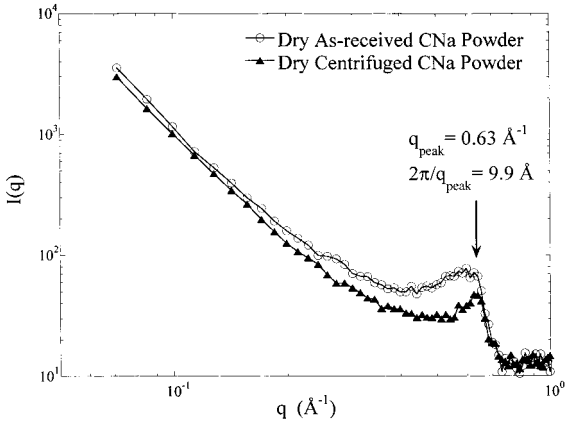

Figure 2. WAXS profiles of as-received and centrifuged CNa dry powders.

tively. If an attractive interaction between the platelets is present, the summation of such an attractive interaction over the large platelet surfaces may give rise to a formation of stacks of parallel platelets (tactoids) as shown in Figure 1c. The contribution of stacked platelets arising from the interplatelet interference to the total coherent scattered intensity is considered as a short-range structure factor, $S_S(q)$, which should be multiplied by $f_c^2(q)$, $f_t^2(q)$, and $f_t(q)f_c(q)$ given in eqs 3a−3c, respectively, to yield the total coherent scattered intensity. Assuming the next neighbor distance in a stack of parallel platelets (tactoids) obeys a Gaussian distribution, the $S_S(q)$ was first calculated by Kratky and Porod to be[22]

$$S_S(q) = 1 + \frac{2}{N}\sum_{k=1}^{N}(N-k)\cos(kDq\cos\varphi) \times \exp[-k(q\cos\varphi)^2\sigma_D^2/2] \quad (4)$$

where φ is the angle between q and the axis of tactoid, N corresponds to the total number of platelets stacked, and D and σ_D represent the next neighbor center-to-center distance and its Gaussian standard deviation (GSD), respectively. Consequently, the total coherent scattered intensity from randomly oriented individual tactoids of parallel clay platelets in dilute dispersions can be written as[26]

$$I_{total}^{CNa}(q) = (\Delta\rho_{CNa})^2\phi_{CNa}V_{CNa}\int_0^{\pi/2} f_c^2(q)S_S(q)\sin\varphi\, d\varphi \quad (5a)$$

for CNa clay platelets and

$$I_{total}^{CNa}(q) = N_{C15A}\int_0^{\pi/2}[\Delta\rho_1(V_t f_t(q) - V_c f_c(q)) + \Delta\rho_c V_c f_c(q)]^2 S_S(q)\sin\varphi\, d\varphi \quad (5b)$$

for C15A clay platelets. The one thing that should be noted is that $S_S(q) = 1$ when $N = 1$. Therefore, eqs 5a and 5b can be reduced to eqs 1 and 2 when $N = 1$.

Results and Discussion

(1) CNa Clays. The spacing of the platelets in dry CNa clays was found to be $2\pi/q_{peak} = 9.9$ Å, where $q_{peak} = 0.63$ Å^{-1}, using WAXS as shown in Figure 2, which is in good agreement with the literature value[1−3] of ca. 10 Å. The centrifuged CNa profile shows a better-defined peak corresponding to 9.9 Å than the as-received one, indicating that the centrifuged CNa material has a better stacking order, probably, because of the relatively slow drying procedure applied compared to commercial processes and/or a narrower distribution in particle size. Both SANS and WAXS data given in Figure 3a indicate that the as-received and the centrifuged CNa clay platelets were both fully exfoliated in deionized water at a concentration of ca. 0.5 wt %. The CNa clay platelets gel in deionized water at a concentration of ca. 2 wt %. Nevertheless, no concentration dependence on the SANS was observed in the CNa clay dispersions with increasing concentration from 0.5 to 4 wt % as shown in Figure 3b. It should be noted that the CNa clay platelets were fully exfoliated in deionized water, although the dispersion/suspension was optically cloudy. The SANS data illustrated in Figure 3b were normalized by $\phi(1-\phi)$, where ϕ is the corresponding volume fraction of clays, and possess a slope of −2.18 ± 0.02, that is, $I(q) \sim q^{-2.18}$, over q ranging from 0.01 to 0.1 Å^{-1}, which is consistent with the reported data[24,27] of ca. −2.2 for Na^+−montmorillonite clays. The single CNa platelet form factor, $P(q)$, calculated using eq 1 with $R = 3000$ Å and $2h = 10$ Å, which were chosen because they are close to those of the clay samples used in this work, possesses a theoretical low-q slope of −2.

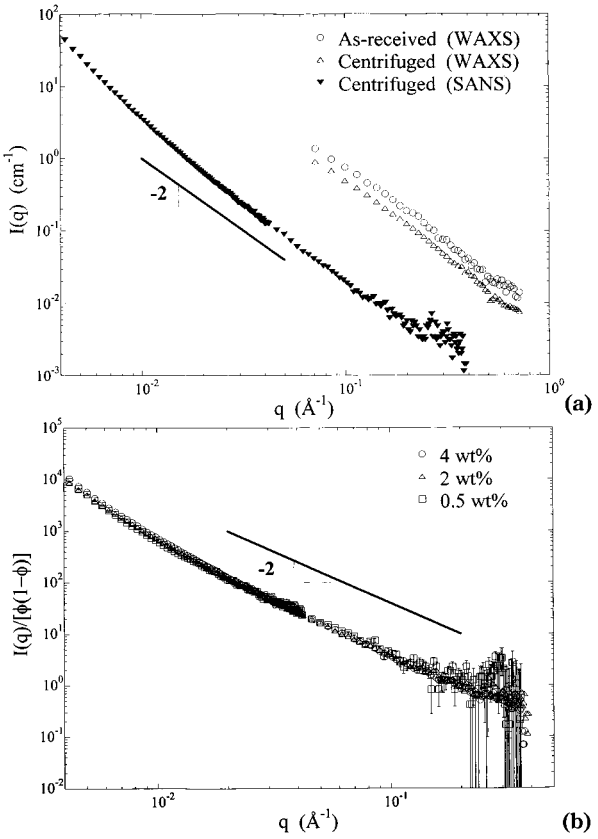

Figure 3. (a) SANS and WAXS profiles of 0.5 wt % as-received and centrifuged CNa platelets dispersed in deionized water. (b) SANS profiles of centrifuged CNa clays dispersed in deionized water at different concentrations. Data were normalized by $\phi(1-\phi)$, where ϕ is the corresponding volume fraction of clays.

(27) Hanley, H. J. M.; Straty, G. C.; Tsvetkov, F. *Langmuir* **1994**, *10*, 3362.

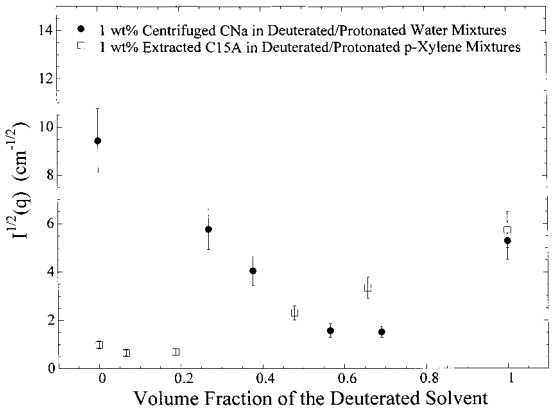

Figure 4. SANS contrast variation experiments on 1 wt % centrifuged CNa and extracted C15A in D_2O/H_2O and d/h *p*-xylene mixtures, respectively. Plot shows the $I^{1/2}(q = 0.0046$ Å$^{-1})$ versus the volume fraction of the deuterated solvent.

The deviation of the measured slope from the theoretical value of −2 could be due to the CNa platelets not being perfectly rigid when dispersed in water.[28]

The neutron SLD of CNa clays was determined to be $(3.9 \pm 0.1) \times 10^{10}$ cm^{-2} by performing SANS contrast variation experiments on the centrifuged CNa clays dispersed at a concentration of 1 wt % in a range of D_2O/H_2O mixtures at room temperature. A contrast-independent slope in the range of q from 0.005 to 0.015 Å^{-1} was found to be -2.20 ± 0.3. The square root of the scattered intensity, $I(q)$, of the first data point at $q = 0.0046$ Å^{-1} in each SANS profile versus the corresponding volume fraction of D_2O is given in Figure 4.

In a brief summary, the CNa clay platelets can be fully exfoliated in deionized water, show no concentration dependence SANS, and possess a contrast- and concentration-independent slope of ca. −2.2 in the SANS profiles in the relatively low-q region.

(2) C15A Clays. The average neutron SLD of C15A clays was determined to be $(1.1 \pm 0.1) \times 10^{10}$ cm^{-2} by performing SANS contrast variation experiments on dispersions of extracted C15A in deuterated/protonated (d/h) *p*-xylene mixtures at concentrations of 0.1 and 1 wt % at room temperature. The scattering profiles of 0.1 and 1 wt % extracted C15A in d/h *p*-xylene mixtures possess a contrast- and concentration-independent slope of -2.38 ± 0.02 over a range of q from 0.008 to 0.04 Å^{-1}. The square root of the scattered intensity of the first data point at $q = 0.0046$ Å^{-1} in each SANS profile versus the corresponding volume fraction of d-*p*-xylene is given in Figure 4 as well.

Figure 5 is the AFM image of single C15A platelets on the Si wafer surface with a vertical dimension (thickness) on the order of ca. 10 Å and lateral dimensions of 0.4−1.0 μm. The WAXS profiles obtained from the dry powder of unextracted and of extracted C15A given in Figure 6 are significantly different, consistent with excess tallow in the unextracted material as reported by the industrial provider. Precipitated tallow was observed in the room temperature waste solvent after the extraction. Extraction likely removes the excess organic modifier (tallow) that is not strongly

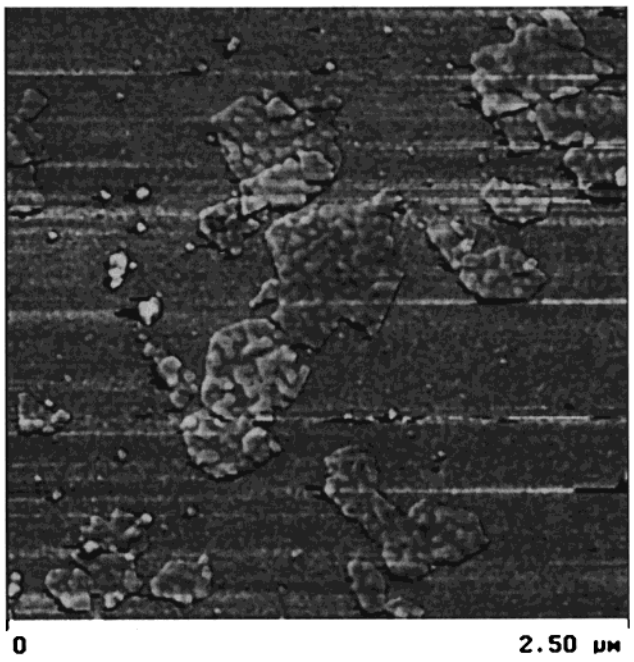

Figure 5. AFM image of individual extracted C15A platelets spun onto an Si wafer surface.

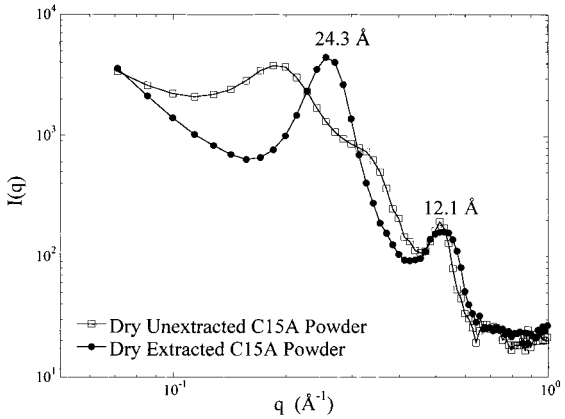

Figure 6. WAXS profiles of unextracted and of extracted C15A dry powders.

bonded to the clay platelet surface. The primary peak (001) for the extracted C15A at $q_{peak} = 0.26$ Å^{-1} corresponds to a platelet spacing of $2\pi/q_{peak} = 24.3$ Å. Assuming a model for the platelet shown in Figure 1a and a core (CNa clay) thickness of 9.9 Å (Figure 2), a single tallow layer on each side of an individual clay platelet in the intercalated tactoids in the dry extracted C15A material has an average thickness of ca. 7.2 Å. It should be noted that the surfactants grafted on opposite surfaces in the interlayer of intercalated clay platelets probably interpenetrate each other, especially in the case of dry organically modified clays.[29] The single tallow layer thickness (d) referred to in this article is simply one-half of the average spacing between adjacent clay platelets in the intercalated tactoids obtained from our measurements and/or data fitting. It does not indicate that the surfactant molecules are collapsed as a layer on each surface with a thickness d. Figure 7 is a comparison of SANS and WAXS data from the

(28) Gilman, J. W.; Jackson, C. L.; Morgan, A. B.; Harris, R. H., Jr.; Manias, E.; Giannelis, E. P.; Wuthenow, M.; Hilton, D.; Phillips, S. H. *Chem. Mater.* **2000**, *12*, 1866.

(29) Hackett, E.; Manias, E.; Giannelis, E. P. *J. Chem. Phys.* **1998**, *108*, 7410.

Table 2. 1 wt % Extracted C15A Dispersed in Deuterated Solvents

	chloroform	benzene	toluene	*p*-xylene
core thickness (Å)	9.9 ± 0.2	9.9 ± 0.3	9.9 ± 0.2	9.9 ± 0.3
layer thickness (Å)	18.6 ± 0.2	17.7 ± 0.5	16.2 ± 0.5	16.1 ± 0.4
GSD of *d*-spacing[a] (Å)	N/A	1.3 ± 0.1	2.8 ± 0.1	3.7 ± 0.1
no. of platelets per tactoid	1	3.0 ± 0.2	2.0 ± 0.2	2.0 ± 0.2

[a] GSD of *d*-spacing represents the Gaussian standard deviation of the spacing of the lamellar tactoid.

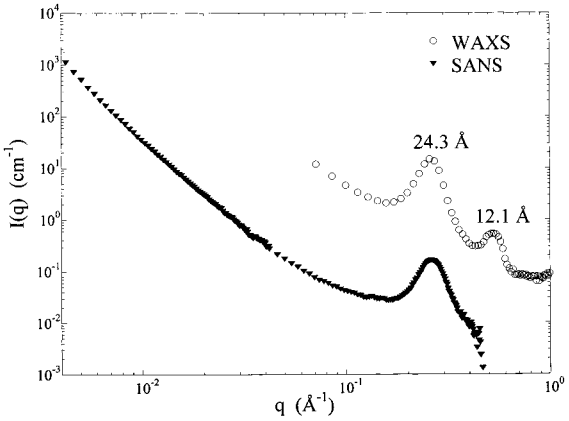

Figure 7. Comparison of SANS and WAXS profiles from the extracted C15A dry powder.

extracted C15A dry powder showing the consistency between these two scattering techniques.

Figure 8a shows the WAXS profiles of 1 wt % extracted C15A dispersed in benzene, toluene, and *p*-xylene. Although the dispersions of extracted C15A in benzene, toluene, and *p*-xylene were optically transparent, the WAXS data indicate that the exfoliation of extracted C15A in the solvents is not complete. Three orders of the primary 46.5-Å spacing are observed for the extracted C15A suspended in benzene and toluene. Assuming the core of the C15A platelets has a thickness of 9.9 Å, the 46.5 Å corresponds to an average single tallow layer thickness of ca. 18.3 Å on each side of an individual clay platelet when dispersed in benzene. These results are consistent with having a swollen tallow layer between the clay platelets. The WAXS profiles from 2 wt % unextracted C15A dispersed in the solvents shown in Figure 8b indicate that the degree of swelling is similar but the peaks are more evident, implying a larger number of platelets per tactoid. In contrast, the WAXS data from 2 wt % unextracted and 1 wt % extracted C15A dispersed in chloroform given in Figure 8c suggest that both the unextracted and extracted C15A platelets were fully exfoliated in chloroform, although the dispersions were optically cloudy.

SANS data of 2 wt % unextracted and 1 wt % extracted C15A dispersed in deuterated (d-) chloroform and the corresponding fitting profiles (solid curves) are presented in Figure 9. According to the WAXS data shown in Figure 8c, both the unextracted and extracted C15A platelets were fully exfoliated in chloroform. Consequently, the SANS data were fitted to the single-platelet form factor for C15A clays (eq 2) over the q ranging from 0.008 to 0.4 Å^{-1} and yield a core (CNa clay) thickness of (9.8 ± 0.3) and (9.9 ± 0.2) Å and a single tallow layer thickness of (17.9 ± 0.3) and (18.6 ± 0.2) Å for the unextracted and extracted C15A dispersed in chloroform, respectively. The parameters of the volume fraction of C15A clays and the SLD of the C15A platelets and of the solvent were known and fixed during the fitting. In the SANS q range (0.004−0.517 Å^{-1}) probed in this work the scattering was not sensitive to the lateral dimension of the C15A platelets. The platelet radius of 3000 Å (0.3 μm) was chosen and fixed for all the fitting and calculations presented in this article. The slope of the SANS profiles in the relatively low-q region (0.008−0.04 Å^{-1}) shown in Figure 9 was found to be −2.20 ± 0.04, that is, $I(q) \sim q^{-2.20}$.

SANS data of 1 wt % extracted C15A dispersed in d-benzene, d-toluene, and d-*p*-xylene and the corresponding fitting profiles (solid curves) are given in Figure 10a. Fitting the SANS data in Figure 10a to eq 5b yields a core (CNa clay) thickness of (9.9 ± 0.3) Å and a tallow layer thickness of (17.7 ± 0.5) Å for extracted C15A dispersed in d-benzene, consistent with the value of 18.3 Å obtained from the WAXS measurements discussed in the previous paragraph. Table 2 gives the fitted parameters for the curves shown in Figures 9 and 10a. From the fits to the SANS data given in Figure 10a the tallow layer thickness (d) decreases while the Gaussian standard deviation (GSD) of the spacing (σ_D) of parallel stacked clay platelets in tactoids increases with decreasing solvent solubility parameter δ, which could explain the diminution of the interplatelet scattering peaks in going from benzene to *p*-xylene as shown in Figure 8a. The increase in d with increasing δ of solvent is consistent with the tallow swelling more as the solubility parameter of the solvent approaches that of the tallow. Figure 10b shows the solvent solubility parameter (δ) versus the tallow layer thickness (d) obtained from fits. A linear fit to the data points illustrated in Figure 10b yields $\delta = (d + 29.1)/2.5$. Assuming that the tallow layer is fully stretched (ca. 26.7 Å in length) when the solubility parameter of the solvent equals that of the tallow, that is, $\delta_{tallow} = \delta_{solvent}$, yields an estimated value of $\delta_{tallow} = 22.3$ (J/m^3)$^{1/2}$, which falls within the literature range[17] of 18−28 (J/m^3)$^{1/2}$. It is interesting that the increase in the swelling of the tallow is coupled with a decrease in the GSD of the interplatelet spacing, indicating that the tactoid is becoming more ordered. While solubility parameters provide some insight into the relative ability of the different solvents to disperse the organically modified clay, they are derived from a bulk property, the energy of vaporization, and it would be more valid to examine local polarizability effects on solvation power (due to the unusual structure of the organically modified clays). Such an analysis is beyond the scope of this article. Figure 10c shows the SANS data of 2 wt % unextracted C15A dispersed in all the d-solvents except d-chloroform given in Table 1. Unlike the SANS data given in Figure 10a, which have a constant slope of ca. −2.38 in the low-q regime (0.008−0.04 Å^{-1}), the slope of the SANS profiles illustrated in Figure 10c varies from ca. −3.26 (benzene) to ca. −2.35 (octane). The strong neutron scattering contrast between the deuterated solvents and

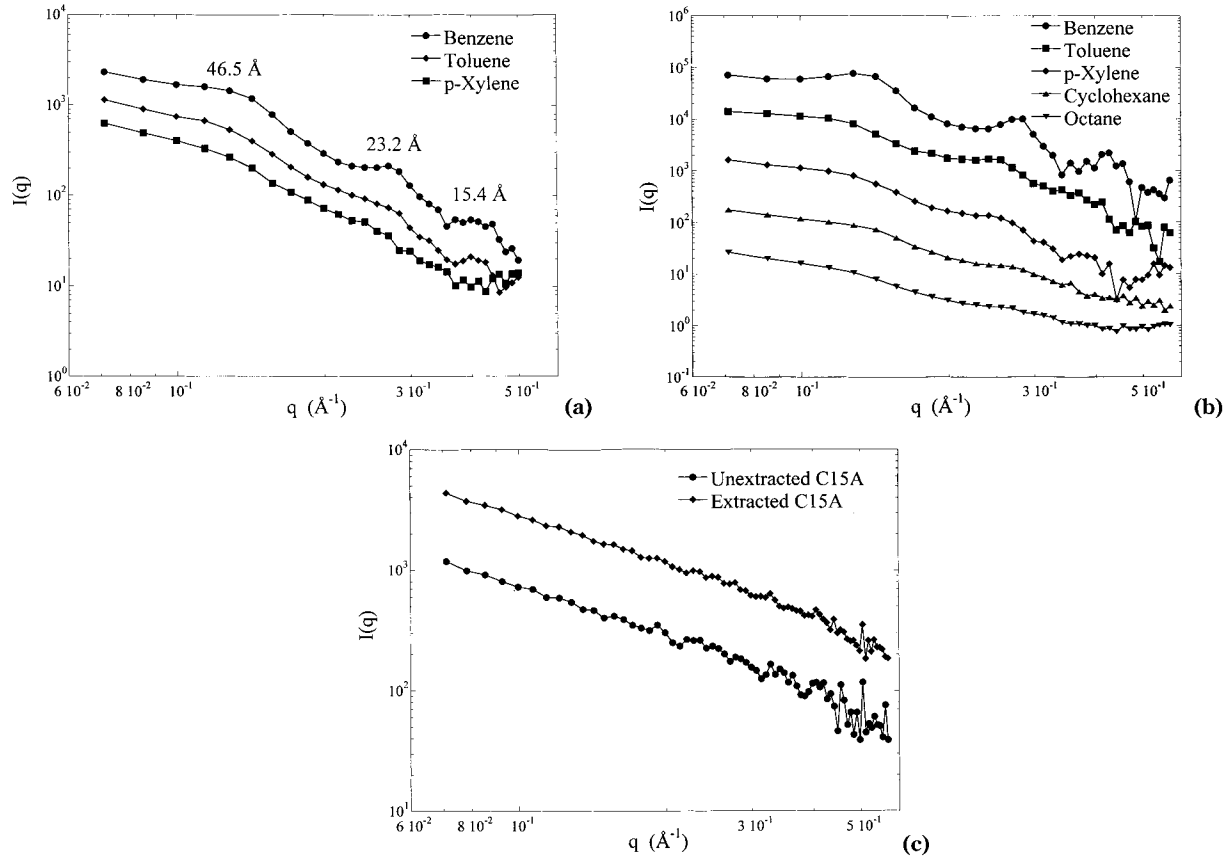

Figure 8. (a) WAXS profiles of 1 wt % extracted C15A dispersed in the organic solvents. (b) WAXS profiles of 2 wt % unextracted C15A dispersed in the organic solvents. (c) WAXS profiles of 2 wt % unextracted and 1 wt % extracted C15A dispersed in chloroform. Profiles are vertically offset for clarity.

Table 3. Extracted C15A Dispersed in Deuterated Toluene

	0.5 wt %	1.0 wt %	2.0 wt %	4.0 wt %
core thickness (Å)	9.9 ± 0.4	9.9 ± 0.2	9.9 ± 0.2	9.9 ± 0.2
layer thickness (Å)	16.4 ± 0.6	16.2 ± 0.5	16.8 ± 0.3	16.6 ± 0.3
GSD of *d*-spacing[a] (Å)	4.6 ± 0.2	2.8 ± 0.1	2.7 ± 0.1	1.3 ± 0.3
no. of platelets per tactoid	2.0 ± 0.2	2.0 ± 0.2	2.0 ± 0.2	2.0 ± 0.2

[a] GSD of *d*-spacing represents the Gaussian standard deviation of the spacing of the lamellar tactoid.

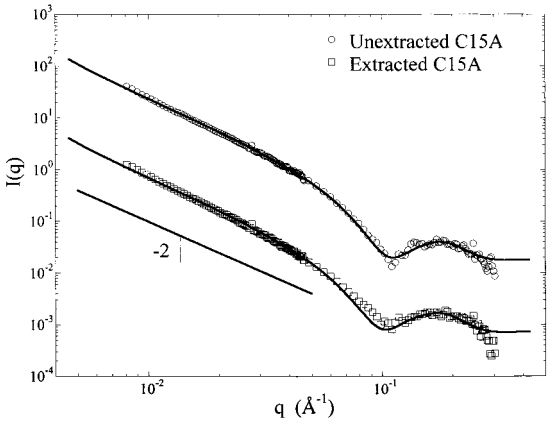

Figure 9. SANS profiles of 2 wt % unextracted and 1 wt % extracted C15A dispersed in d-chloroform. The solid curves are the corresponding fitting profiles. Profiles are vertically offset for clarity.

the protonated tallow, which is absent for X-rays, accounts for the differences in the scattering profiles seen in Figures 8−10, particularly in the range of q = 0.1−0.3 Å^{-1}.

Suspensions of both unextracted and extracted C15A in d-toluene and of extracted C15A in d-chloroform in a range of concentrations were also explored using SANS. The extracted C15A dispersed in d-chloroform does not show any significant concentration dependence on the scattering as shown in Figure 11a, which is similar to the behavior observed from CNa dispersed in deionized water given in Figure 3b, indicating that both unmodified and organically modified clays would not reform tactoids with increasing concentration once the platelets were fully exfoliated in the solvent. The SANS data illustrated in Figure 11a were normalized by $\phi(1 - \phi)$, where ϕ is the corresponding volume fraction of C15A clays. The unextracted C15A dispersed in d-toluene does not show any significant concentration dependence while the extracted C15A exhibits a concentration dependence. The SANS data of the extracted C15A in d-toluene at different concentrations are presented in Figure 11b. Fitting the data given in Figure 11b to eq 5b yields the results listed in Table 3. The parameters given in Table 3 show that the parameters obtained from the single-form factor of C15A given in eq 2 are essentially constant as a function of concentration and

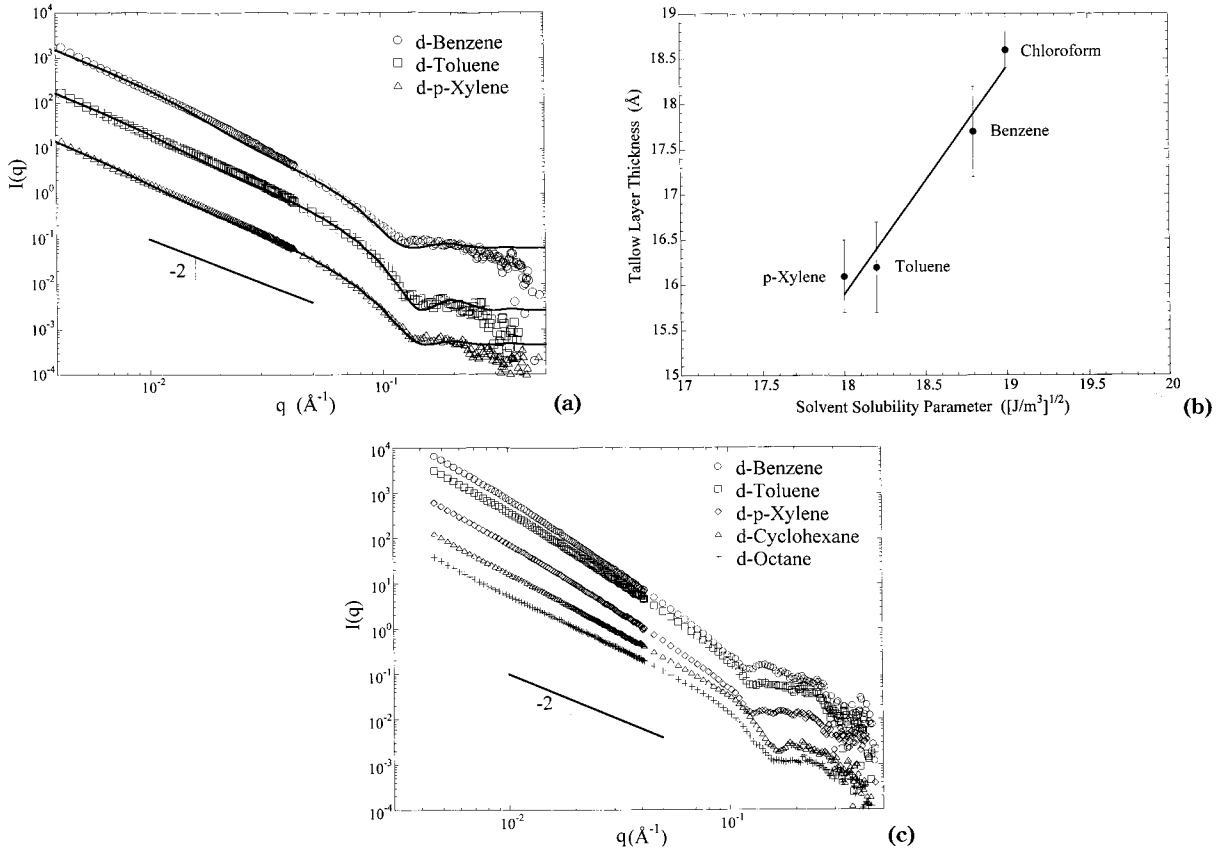

Figure 10. (a) SANS profiles of 1 wt % extracted C15A dispersed in the deuterated solvents. The solid curves are the corresponding fitting profiles. (b) Solvent solubility parameter versus tallow layer thickness obtained from fits. (c) SANS profiles of 2 wt % unextracted C15A dispersed in the deuterated solvents. Profiles are vertically offset for clarity.

that the $S_S(q)$ given by eq 4 changes through an increase in the GSD of the interplatelet spacing of the lamellar tactoid with decreasing concentration. Even the most dilute concentration sample (0.1 wt %) could not be fitted by the single platelet form factor alone. The stacked platelet model (eq 5b) also fails to fit the 0.1 wt % data in the high-q region. Consequently, the SANS data, even at 0.1 wt %, are not a measurement of the single platelet form factor of noninteracting individual C15A platelets. Figure 11b shows a loss of the scattering minimum at ca. $q = 0.14$ Å^{-1} for the 0.1 wt % sample. This minimum is due to oscillations in $P_t(q)$ (eq 3b), arising from overall platelet thickness. The disappearance of this minimum could be due to two different possible reasons: (1) a distribution in thickness of the organically modified clay platelets or (2) a smooth neutron scattering length density transition from the surfactant layer into the solvent (i.e., not a step function change). The thickness of the clay platelet is very uniform and it is likely that the transition from the organic layer to the solvent is a smoothly varying profile as seen for a polymer brush in a good solvent. The surfactant/solvent interface will also be smeared somewhat by the different chain lengths present in the ditallow. The scattering profiles of extracted C15A in d-toluene shown in Figure 11b exhibit a concentration-independent slope of -2.36 ± 0.04, that is, $I(q) \sim q^{-2.36}$, in the q range from 0.008 to 0.04 Å^{-1}, similar to the slope obtained from the dispersions of 1 wt % extracted C15A in benzene and in *p*-xylene (Figure 10a) reported earlier in this article.

The low-q slope of the calculated coherent scattered intensity using eq 5b and the fitted parameters for 1 wt % extracted C15A in d-toluene given in Table 2 increases with increasing value of N (number of platelets stacked per tactoid) as shown in Figure 12. For instance, the calculated single platelet form factor, $P(q)$, with $N = 1$ and $I(q)$ with $N = 20$ for C15A clays possess a slope of -2.1 and -2.9 in the low-q regime, respectively. The $I(q)$ with $N = 2$ in Figure 12, which possesses a low-q slope of -2.36, is the fitted curve for the toluene data presented in Figure 10a. The only variable for the calculated $P(q)$ and $I(q)$ is the value of N, suggesting that the deviation of slope from -2.1 mainly arises from stacking of clay platelets. The low-q slope increases while the absolute scattered intensity of the peak in the oscillation of the form factor near $q = 0.2$ Å^{-1} decreases with increasing N, which consequently, might be used to determine the N value. The slope of the calculated $P(q)$ for C15A platelets (-2.1) is close to that of $P(q)$ calculated for CNa platelets (-2.0) using eqs 2 and 1 for ideal thin disks with and without an absorbed surfactant layer, respectively. Consequently, the slope of fully exfoliated C15A platelets in organic solvents would be expected to be close to that of fully exfoliated CNa platelets in deionized water, which has been confirmed by the SANS measurements illustrated in Figures 3b and 9. The single platelet form factors of C15A and CNa clays were obtained from fully exfoliated clay platelets dispersed in chloroform and water, respectively, and consequently yield the same low-q slope of ca. -2.2.

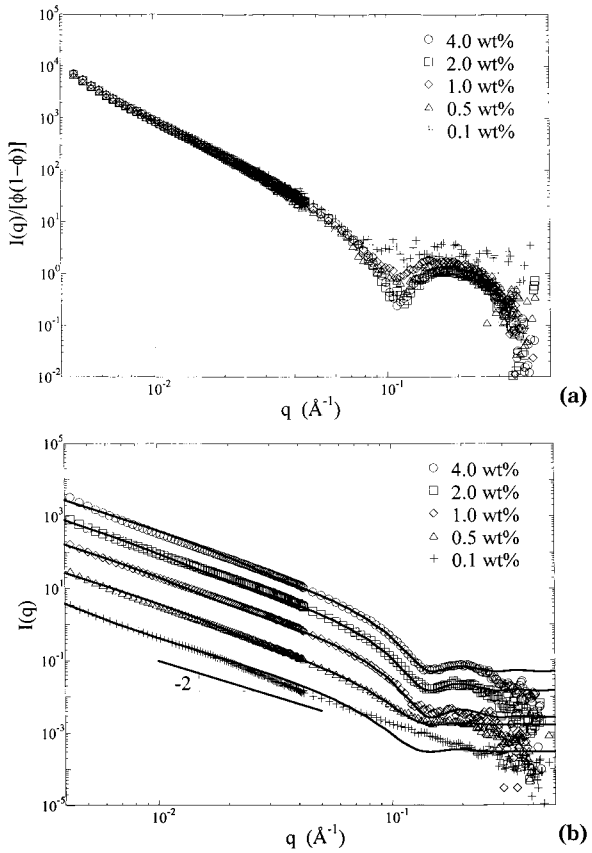

Figure 11. (a) SANS profiles of extracted C15A dispersed in d-chloroform in a range of concentrations. Data were normalized by $\phi(1 - \phi)$, where ϕ is the corresponding volume fraction of clays. (b) SANS profiles of extracted C15A in deuterated toluene in a range of concentrations. The solid curves are the corresponding fitting profiles. Profiles are vertically offset for clarity.

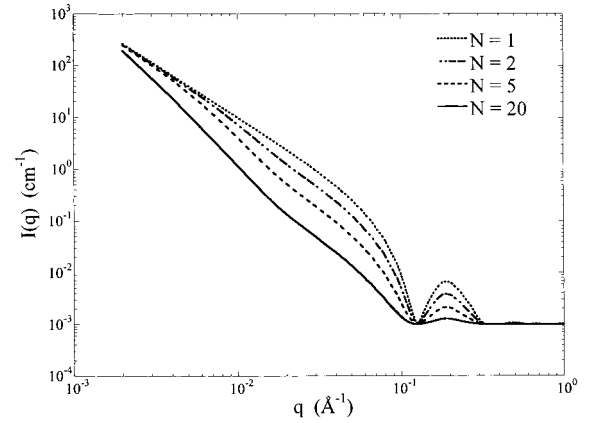

Figure 12. Calculated $I(q)$ with different values of N, the number of clay platelets per tactoid, using eq 5b and the fitted parameters for 1 wt % extracted C15A in d-toluene given in Table 2.

Experiments of temperature dependence on dispersions of 1 wt % extracted C15A in d-toluene at 25 and 60 °C and in d-chloroform at 5, 25, and 45 °C were performed using SANS as well. Nevertheless, no evidence of any temperature dependence on the scattering was observed.

Conclusions

The structure of unextracted and extracted organically modified montmorillonite clays dispersed in a variety of solvents was characterized using SANS and WAXS techniques. It was confirmed that the organic modifier is present in significant excess in the unextracted material. Dispersions of both unextracted and extracted C15A platelets in chloroform exhibited scattering characteristic of independent disk-like particles, with a low-q slope of ca. −2.2, indicating that the material is fully exfoliated. The C15A clays swell but retain vestiges of their lamellar structure in benzene, toluene, and *p*-xylene while the platelets aggregate to form large particles in cyclohexane and octane. A model for the clay/tallow (core/layer) structure has been established to fit the SANS data presented and the fitted parameters indicate that the thickness of the tallow layer increases while the Gaussian standard deviation of the next neighbor center-to-center distance between stacked platelets decreases with increasing solvent solubility parameter. The extracted C15A dispersed in chloroform does not show any concentration dependence on the scattering within the range of concentrations studied in this work. The extracted C15A dispersion in toluene exhibits a concentration dependence on the scattering while the unextracted C15A dispersion does not. A contrast and concentration-independent slope of ca. −2.36 was observed in the low-q region in all the SANS profiles obtained from the dispersions of extracted C15A in benzene, toluene, and *p*-xylene, suggesting that the deviation of slope from the theoretical value of −2.1 may arise from stacking of clay platelets. Unextracted C15A is more readily suspended (i.e., shows less tendency to gel or form precipitates) than extracted C15A in the organic solvents studied. This is consistent with the industrial practice of adding excess surfactant to clays to promote the solvation kinetics (and prevent gelation) in organic solvents. The scattering data suggest that the unextracted material disperses as larger tactoids, which interact weakly and hence tend to remain suspended.

Acknowledgment. The authors acknowledge the support of the NIST, U.S. Department of Commerce, and the National Science Foundation, through Agreement No. DMR-9986442, in providing the neutron research facilities used in this work. We thank Prof. R. Krishnamoorti at the University of Houston and Dr. B. Hammouda at the NIST for many helpful discussions and suggestions and Dr. X. Gu in the Building and Fire Research Laboratory (BFRL) at the NIST for the AFM measurements. The authors also thank one of the reviewers for insightful comments on the manuscript.

CM0008617